Chemical Science

EDGE ARTICLE

View Article Online
View Journal | View Issue

Cite this: *Chem. Sci.*, 2017, **8**, 4306

Coupling functionalized cobalt ferrite nanoparticle enrichment with online LC/MS/MS for top-down phosphoproteomics†

Bifan Chen, ‡[a] Leekyoung Hwang,‡[a] William Ochowicz,[a] Ziqing Lin,[b] Tania M. Guardado-Alvarez,[a] Wenxuan Cai,[b] Lichen Xiu,[a] Kunal Dani,[a] Cyrus Colah,[b] Song Jin *[a] and Ying Ge *[abc]

Received 12th December 2016
Accepted 30th March 2017

DOI: 10.1039/c6sc05435h

rsc.li/chemical-science

Phosphorylation plays pivotal roles in cellular processes and dysregulated phosphorylation is considered as an underlying mechanism in many human diseases. Top-down mass spectrometry (MS) analyzes intact proteins and provides a comprehensive analysis of protein phosphorylation. However, top-down MS-based phosphoproteomics is challenging due to the difficulty in enriching low abundance intact phosphoproteins as well as separating and detecting the enriched phosphoproteins from complex mixtures. Herein, we have designed and synthesized the next generation functionalized superparamagnetic cobalt ferrite ($CoFe_2O_4$) nanoparticles (NPs), and have further developed a top-down phosphoproteomics strategy coupling phosphoprotein enrichment enabled by the functionalized $CoFe_2O_4$ NPs with online liquid chromatography (LC)/MS/MS for comprehensive characterization of phosphoproteins. We have demonstrated the highly specific enrichment of a minimal amount of spike-in β-casein from a complex tissue lysate as well as effective separation and quantification of its phosphorylated genetic variants. More importantly, this integrated top-down phosphoproteomics strategy allows for enrichment, identification, quantification, and comprehensive characterization of low abundance endogenous phosphoproteins from complex tissue extracts on a chromatographic time scale.

Introduction

Reversible protein phosphorylation orchestrates important cellular processes in eukaryotic cells including cell proliferation, protein–protein interaction, signal propagation, among others.[1,2] Dysregulation of protein phosphorylation is known to be critically involved in the pathogenesis of many human diseases, such as cancer, heart failure, and neurodegenerative disease.[1,3–7] To understand these disease processes, identification and quantification of phosphoproteins are the essential steps in decoding the complex cellular signaling network regulated by phosphorylation events. Moreover, proteoforms arising from alternative splicing, amino acid polymorphisms, and other post-translational modifications (PTMs),[8] have imposed another layer of complexity to the phosphoproteome. The conventional shotgun "bottom-up" mass-spectrometry (MS) based phosphoproteomics which analyzes peptides resulted from protein digestions,[9,10] is suboptimal because of the "protein inference problem", resulting in incomplete information on sequences or modifications.[11,12] In contrast, the top-down MS approach examines intact proteins without digestion, providing a global view and the possible merit of comprehensive analysis of all modified proteoforms.[5,13–16] Therefore, top-down MS allows one to study phosphoproteins and their associated proteoforms at the intact protein level, which leads to more direct connectivity to complex disease phenotypes for clinical and translational research.[11]

However, unlike the well-established bottom-up phosphoproteomics that has numerous mature phosphopeptide enrichment methods and well-developed LC/MS/MS workflows,[17–19] the top-down phosphoproteomics approach is much more challenging mainly due to the lack of phosphoprotein enrichment methods and the difficulties in separation of intact proteins from complex proteome. To address the limitation of low specificity, efficiency, and poor reproducibility on intact protein enrichment,[20–23] we recently developed the first generation functionalized superparamagnetic Fe_3O_4–GAPT-Zn nanoparticles (NPs) for universal and effective enrichment of phosphoproteins from complex mixtures.[24] However, further improvement on the NPs and effective downstream analysis including LC separation and MS/MS characterization of

[a]*Department of Chemistry, University of Wisconsin–Madison, Madison, WI, USA. E-mail: ge2@wisc.edu*

[b]*Department of Cell and Regenerative Biology, University of Wisconsin–Madison, Madison, WI, USA*

[c]*Human Proteomics Program, School of Medicine and Public Health, University of Wisconsin–Madison, Madison, WI, USA*

† Electronic supplementary information (ESI) available: Material and methods, characterization of the NPs, and top-down MS. See DOI: 10.1039/c6sc05435h

‡ These authors contributed equally to this work.

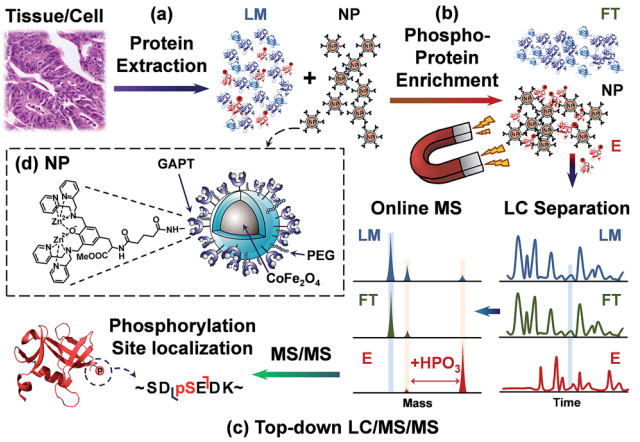

Fig. 1 Schematic illustration of the top-down phosphoproteomics strategy integrating intact phosphoprotein enrichment using functionalized magnetic nanoparticles (NPs) with online LC/MS/MS. (a) Proteins were extracted from tissue (or cell), and subjected to enrichment by functionalized $CoFe_2O_4$ NPs. (b) Phosphoproteins bound on magnetic NPs were then pulled down by a magnet for subsequent elution. (c) The loading mixture (LM), flow through (FT), and elution (E) were further separated and analyzed by top-down LC/MS. Enriched phosphoproteins are then comprehensively characterized by online LC/MS/MS. (d) Details of the $CoFe_2O_4$ NPs functionalized with GAPT-Zn ligands that specifically bind to phosphate groups.

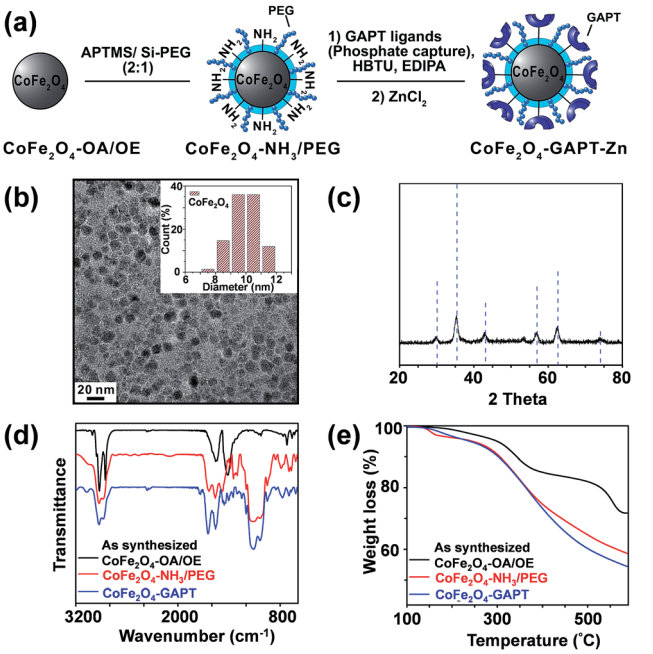

Fig. 2 (a) Schematic illustration of the synthesis of functionalized $CoFe_2O_4$ NPs. The GAPT-Zn chelating groups possess strong binding ability and preference for phosphate dianions at neutral pH. (b) TEM image of as-prepared $CoFe_2O_4$–OA/OE NPs. Inset shows the size distribution (9.96 ± 1.03 nm) of the NPs. (c) PXRD pattern of as-synthesized $CoFe_2O_4$–OA/OE NPs. Blue dash lines indicate a typical diffraction pattern of a ferrite structure. (d) FTIR and (e) TGA analysis of as-synthesized $CoFe_2O_4$–OA/OE (black), functionalized $CoFe_2O_4$–NH_3/PEG (red), and functionalized $CoFe_2O_4$–GAPT (blue) NPs.

enriched phosphoproteins are needed to fully interrogate the complex phosphoproteome.

Herein, we sought to develop a robust top-down proteomics workflow for comprehensive phosphoprotein characterization that integrates highly specific intact phosphoprotein enrichment by the next generation cobalt ferrite ($CoFe_2O_4$) NPs with high resolution online LC/MS/MS analysis (Fig. 1). In this top-down phosphoproteomics workflow, proteins are first extracted from tissue homogenate (or cell lysate), and subsequently incubated with functionalized superparamagnetic NPs (Fig. 1a). At a neutral pH, the ligands functionalized on the NP surface bound strongly to phosphate groups of the phosphoproteins, preserving their physiological condition (Fig. 1b). After a magnetic pull down of the phosphoprotein-bound NPs, elution of the phosphoproteins from NPs (as well as the pre-enrichment samples) are then subjected to online LC separation and MS analysis of the intact proteins. The enriched phosphorylated species are selected for tandem MS for identification and characterization (Fig. 1c). For the first time, we have shown that this integrated top-down phosphoproteomics strategy allows for highly specific enrichment, identification, quantification, and comprehensive characterization of low abundance endogenous phosphoproteins from complex tissue extracts on a chromatographic time scale.

Results and discussion

Synthesis, characterization, and evaluation of $CoFe_2O_4$ NPs for intact phosphoprotein enrichment

We have designed and synthesized the cobalt ferrite ($CoFe_2O_4$) NPs (Fig. 1d and 2a) with stronger magnetic response[25,26] and better reproducibility for intact phosphoprotein enrichment than the first generation Fe_3O_4–GAPT-Zn NPs.[24] We synthesized the $CoFe_2O_4$ NPs capped with oleic acid (OA) and oleylamine (OE) ligands by a seed-mediated growth method (see experimental details in ESI and Fig. S1†) following the procedure reported by Sun *et al.*[27] Transmission electron microscopy (TEM) image analysis revealed that the diameter of the $CoFe_2O_4$ NPs was ~9.96 ± 1.03 nm (Fig. 2b). Powder X-ray diffraction confirmed a typical ferrite diffraction pattern[28] (Fig. 2c). The $CoFe_2O_4$ NPs have been shown to possess larger magnetic moments and magnetic anisotropy and good chemical stability.[25,26] These NPs were subsequently functionalized with dinuclear Zn(II)-dipicolylamine (Zn-DPA) ligands coupled to glutaric acid (hereafter referred to as GAPT), based on the previously reported method with minor modifications (Fig. 2a).[24] These GAPT-Zn complexes provide the specific binding to the phosphate ions on phosphoproteins and are the key to the enrichment.[24,29] Notably, the step that replaces the hydrophobic OA and OE ligands on the $CoFe_2O_4$ NP surface with 3-aminopropyl trimethoxy silane (APTMS) and 2-methoxyl (polyethyleneoxy) propyl trimethoxysilane (hereafter referred to as Si-PEG) was completed within 24 h, which was greatly improved compared to 48 h for the preparation of Fe_3O_4–NH_3/PEG NPs.[24] We then coupled GAPT ligands, the phosphate capturing moiety, to the free amino groups of the APTMS on $CoFe_2O_4$–NH_3/PEG NPs, producing $CoFe_2O_4$–GAPT NPs. Fourier

transform infrared spectroscopy (FTIR) indicating strong band around 1147–1028 cm^{-1}, peaks around 1200 cm^{-1} (Si–O-R, C–O–C, EO CH_2), and sharp peak around 1650 cm^{-1} for $CoFe_2O_4$–GAPT (amide bond), and thus confirmed the proper functionalization of the NPs with the ligand molecules (Fig. 2d).[30] Additionally, thermogravimetric analysis (TGA) showed different weight loss (%) for each surface-modified $CoFe_2O_4$ NPs with the corresponding ligand molecules (Fig. 2e). The small size of the $CoFe_2O_4$ NPs provides advantages such as a high surface-to-volume ratio, easy surface functionalization with multivalent ligand molecules to interact with phosphoprotein targets; better penetrations in complex mixture for higher binding rate without causing denaturation; and good solubility.[31–33]

After activation of $CoFe_2O_4$–GAPT NPs with 10 mM $ZnCl_2$, the resulting $CoFe_2O_4$–GAPT-Zn NPs (Fig. 1d) were used for phosphoprotein enrichment. The protein samples prior to NP enrichment were termed loading mixture (LM); unbound non-phosphoproteins were collected as flow-through (FT); and enriched phosphoproteins were saved as elution (E) for further analysis (Fig. 1c). The optimized enrichment procedure includes a HEPES buffer (50 mM, pH 7.7, 150 mM NaCl) for binding and subsequent washing, and a sodium phosphate (Na_2HPO_4) buffer (100 mM, pH 7.3, 50 mM NaCl) for final elution. A standard protein mixture was used to validate the enrichment efficacy of each batch of NPs (details in ESI, Fig. S2a and b†). We further sought to quantitatively determine the enrichment performance by spiking in low levels of β-casein as an internal control in a highly complex swine heart tissue extract. We systematically decreased the concentration of the spike-in β-casein from 0.1 to 0.03 μg μL^{-1}. 10 μg of equal amount of proteins before and after enrichment of the tissue extract containing about 3% (I), 5% (II), 7% (III), and 10% (IV) w/w % of β-casein (Table S1†) was prepared as loading mixtures. SDS-PAGE analysis was performed (Fig. 3a and b, and S3†) paralleled to the top-down LC/MS analysis (*vide infra*).

Overall, the enrichment was consistent and reproducible across all samples with different amounts of spike-in β-casein.

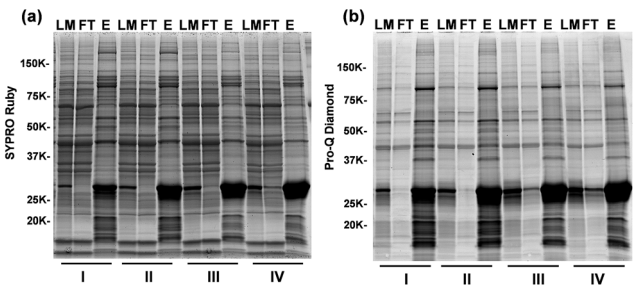

Fig. 3 SDS-PAGE analysis with (a) Sypro Ruby and (b) Pro-Q Diamond based detection of spike-in β-casein and other endogenous phosphoproteins specifically enriched from highly complex swine heart tissue extracts (loading mixture). Each loading mixture (LM) contains different concentration of 0.03 μg μL^{-1} (I), 0.05 μg μL^{-1} (II), 0.07 μg μL^{-1} (III), and 0.1 μg μL^{-1} (IV) of spiked-in β-casein. Equal amount (10 μg) of the loading mixture, flow-through (FT), and elution after enrichment (E) was loaded on the gel. M: marker; LM: loading mixture; FT: flow through; E: elution.

Abundant non-phosphoproteins in LM were effectively depleted and washed into FT, as shown in the nearly identical bands between LM and FT (Fig. 3a). In contrast to LM and FT, the highly similar band patterns in the elution (E) lanes of the gel stained by Sypro Ruby and ProQ Diamond (Fig. 3a and b) indicates the predominance of enriched endogenous phosphoproteins in addition to β-casein. These results demonstrated that $CoFe_2O_4$–GAPT-Zn NPs can efficiently enrich phosphoproteins from complex biological samples with high specificity and sensitivity.

Top-down LC/MS analysis of spike-in β-casein from tissue extract after $CoFe_2O_4$ NPs enrichment

For the top-down proteomic analysis after NP enrichment, an equal amount of proteins from LM, FT, and E that were acquired from the tissue extract with 5% of β-casein spike-in was subjected to reverse phase chromatography (RPC) LC/MS and LC/MS/MS analyses using a Waters M-class UPLC and a Bruker maXis II Q-TOF mass spectrometer (details in ESI†). The robust LC/MS platform allows direct comparison across the base peak chromatograms (BPC) of LM, FT, and E (Fig. 4a). The overlapping separation pattern between LM and FT (Fig. 4a and S4†) demonstrates that the majority of the proteins from LM were washed off to FT, consistent with the SDS-PAGE band patterns (Fig. S3†). Subsequent MS analysis revealed that most proteins in the LM and FT solutions are highly abundant non-phosphoproteins, including blood proteins such as hemoglobin subunit α and β, which were significantly depleted after enrichment (Fig. S5 and S6†). Even though some blood proteins were still detected in MS from elution, significant depletion of highly abundant non-phosphoproteins in LM enabled us to detect low abundance phosphoproteins in E, which are reflected as low abundance peaks in the BPC for E. For example, the deconvoluted spectrum shows that the spike-in β-casein was barely detectable in LM and FT solutions because of the predominant signal from the co-eluting myoglobin (Fig. 4b). However, after enrichment using $CoFe_2O_4$–GAPT-Zn NPs, β-casein (M_r 23 968.12) was significantly enriched while the intensity of myoglobin (M_r 16 942.86) was greatly decreased (Fig. 4b). The enrichment factor was estimated by comparing the relative percentage of β-casein before and after the enrichment. The relative percentage of β-casein was significantly increased from 0.5% to 94% from the complex mixture after enrichment. Moreover, the pure spike-in β-casein standard were separated into three distinct LC peaks in E after enrichment, as seen in the BPC and extracted ion chromatogram labeled as (i), (ii), and (iii) in Fig. 4a. None of these were detectable prior to enrichment in LM. The deconvoluted mass spectra revealed three genetic variants of β-casein,[34] B (M_r 24 077.14); (i), A1 (M_r 24 008.11); (ii), and A2 (M_r 23 968.12); (iii) based on their accurate mass measurement (Fig. 4c and S7†). Although the genetic variants of β-casein differ by only one or two amino acid residues, all three proteoforms were unbiasedly enriched by the NPs and separated from the complex tissue extract using top-down LC/MS. Furthermore, the top-down approach allowed us to quantify the relative percentage of each β-casein proteoform,

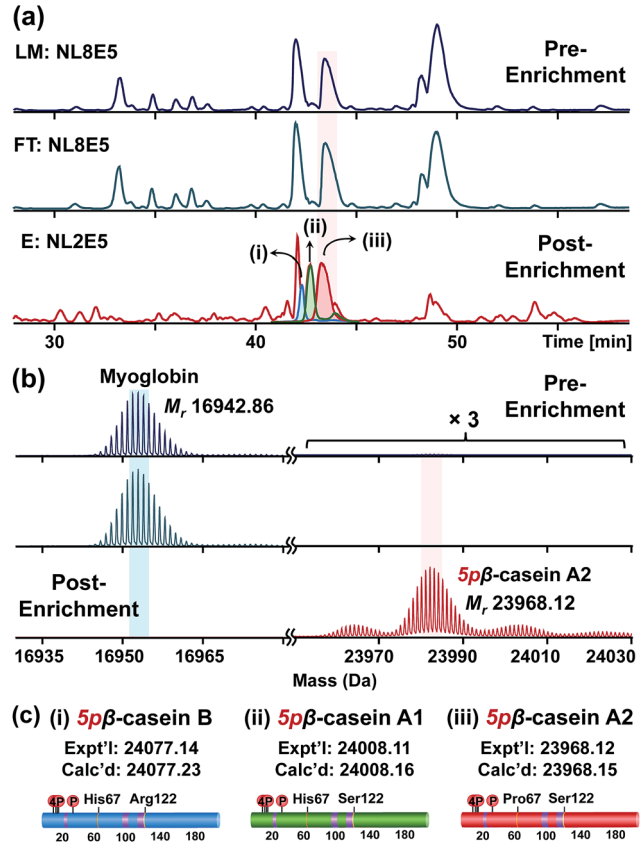

Fig. 4 Top-down LC/MS analysis of multiple β-casein variants after phosphoprotein enrichment from a swine heart tissue extract with 0.05 μg μL^{-1} of spike-in β-casein. (a) Base peak chromatograms of LM (loading mixture; dark blue), FT (flow through; light blue), and E (elution; red). (i), (ii), and (iii), represent extracted ion chromatograms of β-casein variants. (b) Average mass spectra and deconvoluted spectra of LM (dark blue), FT (light blue), and E (red) samples from 41.3 to 41.7 min (highlighted in grey). The intensity in the region from 23 940 Da to 24 040 Da was magnified 3 times. NL: normalized level. (c) Cartoon illustration of the three β-casein variants B (i), A1 (ii), and A2 (iii), each carrying five phosphorylations.

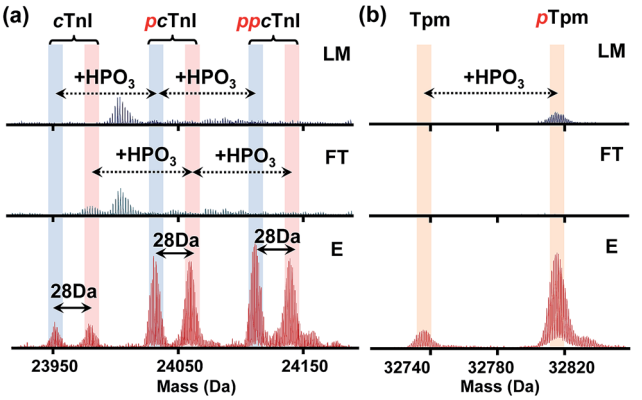

Fig. 5 LC/MS detection of well characterized cardiac phosphoproteins enabled by highly specific NP-based enrichment from a complex tissue extract. Representative endogenous phosphoproteins, (a) cardiac troponin I (cTnI) and (b) tropomyosin (Tm) were shown by comparing normalized deconvoluted average MS spectra of loading mixture (LM), flow through (FT), and elution from 37.5–37.8 min and 41.3–41.4 min, respectively. Mass difference of 28 Da corresponding to polymorphism V116A was observed for cTnI.

which would be difficult using the bottom-up MS strategy. The relative percentages among A2, A1, and B variants were determined to be 53%, 35% and 12% respectively, according to the average spectrum across the same time frame (Fig. S8†).

Top-down LC/MS/MS characterization of endogenous phosphoproteins enriched from tissue extract by $CoFe_2O_4$ NPs

Furthermore, through this integrated top-down phosphoproteomics strategy, we have detected and examined multiple known cardiac phosphoproteins[7] from the eluted phosphoproteins that were previously undetected or in very low abundance in the HEPES extraction without enrichment (Fig. 5). The enrichment of the phosphoproteins is apparent by comparing phosphorylation level changes across the same time frame in the LC/MS of LM, FT, and E. Notably, as shown in the normalized deconvoluted spectra in Fig. 5a, phosphorylated forms of pig cardiac troponin I (24 kDa) with a possible V116A polymorphism (28 Da) were all enriched, which was consistent with what we previously found on the same protein using immunoaffinity purification.[35] Western blot analysis for phosphorylated cardiac troponin I at Ser22/23 further demonstrated the enrichment (Fig. S9†), which well correlates with the MS data. Nevertheless, the top-down approach in this case offers a global view of each of these highly similar phosphorylated polymorphic species. Similarly, phosphorylated tropomyosin (33 kDa) was also enriched and can be characterized after enrichment (Fig. 5b).

More importantly, in addition to the previously known myofilament proteins, we were able to discover low abundance endogenous phosphoproteins using this integrated strategy. One example is a potential phosphoprotein (27 kDa) eluting around 33.5 min that was significantly enriched so that the triply phosphorylated form became the most intense peak/base peak (Fig. 6a). The deconvoluted spectrum further shows that the protein with M_r 26 996.90 has 80 Da mass increases, corresponding to multiple phosphorylated forms of the protein (Fig. 6b). As seen in both the original and the deconvoluted spectra, the triply phosphorylated form was of very low abundance in LM of the heart tissue extract, but after enrichment, its intensity improved more than 10 folds (Fig. 6a and b). Moreover, nearly no detection of the phosphorylated forms in FT spectra demonstrates sufficient capturing ability of the $CoFe_2O_4$–GAPT NPs. Since the triply phosphorylated form became the base peak after enrichment, subsequent LC/MS/MS was made possible through both collision-induced dissociation (CID) and electron transfer dissociation (ETD).

We confidently identified this protein as hepatoma-derived growth factor (UniProtKB/Swiss-Prot, F1RHJ2_PIG) using MS-Align+[36,37] search algorithm (Fig. S10†), which was previously uncharacterized and unreviewed. We further analyzed the data and mapped the sequence using MASH suite Pro.[37] Three potential phosphorylation sites were determined: Ser132, Ser133, and Ser165 (red letters in Fig. 6c and S11†). Top-down

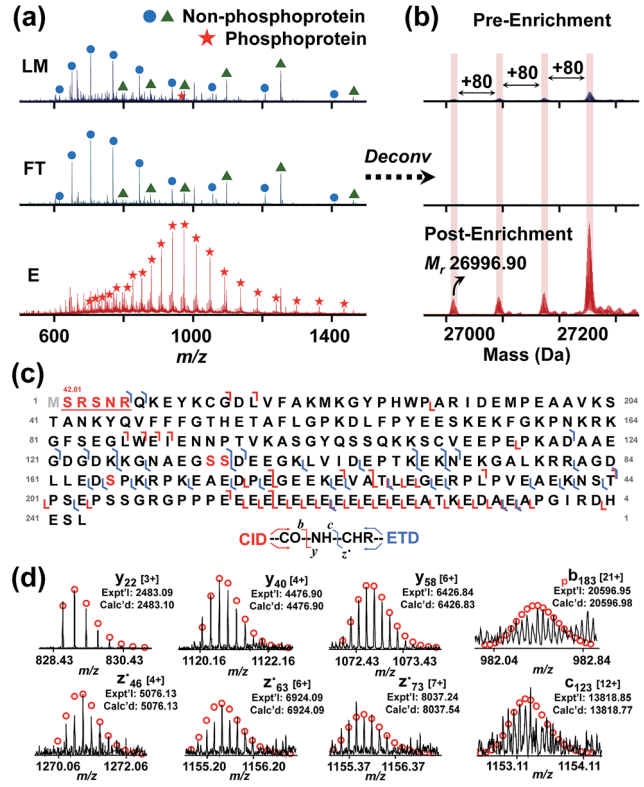

Fig. 6 LC/MS/MS analysis of a representative previously uncharacterized phosphoprotein, hepatoma-derived growth factor, enabled by effective $CoFe_2O_4$ NP-based enrichment from a complex swine heart tissue extract. (a) MS spectra of loading mixture (LM, dark blue), flow through (FT, light blue), and elution (E, red) from 32.3 min to 32.7 min; (b) the corresponding deconvoluted spectra. (c) Fragment ion map of online MS/MS analysis with CID and ETD from triply phosphorylated precursor ion (29+). Grey "M" indicates methionine excision and red "S" indicates phosphorylation sites. Red numbers above the underlined red sequence reveal modifications with their additional mass. (d) Representative fragment ions from both online CID and ETD LC/MS/MS of the targeted protein.

MS/MS not only revealed an N-terminal methionine excision, but also a coexisting acetylation near the N-terminal in addition to the three phosphorylations. As another example, a protein with M_r 21 675.63 with a mass increase of 80 Da was significantly enriched and detected in E (Fig. S12a†), while it was nearly unobservable in LM and FT. In the normalized original mass spectra in Fig. S12a,† the non-phosphoprotein with M_r 20 827.56 was fully depleted, and the phosphorylated protein M_r 21 675.63 + 80 Da was enriched more than 10 folds, demonstrating the specificity of this NP-based enrichment and the efficacy of this integrated strategy. MS-Align + search identified the proteins to be chromobox protein homolog 1 (UniProtKB/Swiss-Prot, F1RWH1_PIG) based on both the CID and ETD spectra acquired from LC/MS/MS and we narrowed down the possible phosphorylation site to Ser89/Ser91 (Fig. S12 and S13†). Similarly, we enriched and identified a 14 kDa singly phosphorylated protein, programmed cell death protein 5 (UniProtKB/Swiss-Prot, F1RNX2_PIG) (Fig. S14 and S15†). Interestingly, even though phosphorylation is known as a labile PTM, many of the phosphorylations were preserved during CID LC/MS/MS (Fig. 6d, S12d and S16†). For instance, from the phosphoprotein with M_r 21 755.59, $_p$y121 ion was predominantly observed whereas its unphosphorylated counterpart y121 existed in low abundance (Fig. S16†). The globular structure of intact proteins preserves the labile phosphorylation to some degree.[16] Other enriched phosphoproteins with observable 80 Da mass difference were also detected in the comparison among LM, FT, and E (Fig. S17†). These results in the identification and characterization of new phosphoproteins not only validated the enrichment performance of the $CoFe_2O_4$–GAPT-Zn NPs but also demonstrated the power of this integrated top-down phosphoproteomics workflow.

Conclusions

In summary, we have developed a top-down phosphoproteomics strategy that integrates NP-based phosphoprotein enrichment and online LC/MS/MS to enrich, identify, quantify, and characterize phosphoproteins from complex protein mixtures. We have designed and synthesized functionalized magnetic $CoFe_2O_4$–GAPT-Zn NPs with stronger magnetic response and much improved robustness and reproducibility in synthetic steps. The high specificity and efficiency of phosphoprotein enrichment using these improved $CoFe_2O_4$–GAPT-Zn NPs was validated by SDS-PAGE analysis with phosphoprotein-specific gel stains using β-casein spike-in tissue extract. Top-down LC/MS results demonstrated that the spike-in phosphorylated β-casein was substantially enriched (relative percent from 0.5% to 94%), which allowed us to further separate, identify, and quantify all of its genetic variants. More importantly, through online top-down LC/MS/MS with CID and/or ETD, we were able to identify endogenous phosphoproteins and localize their potential phosphorylation sites. Benefiting from the unique NP-based enrichment method, this integrated online top-down LC/MS/MS workflow has the advantages of globally observing phosphorylated proteoforms; quantifying proteoform species; and identifying and characterizing phosphoproteins with co-existing PTMs and/or sequence variants. We envision that with further advances in front-end intact protein separation,[38] MS detection of large proteins (>30 kDa), and MS/MS fragmentation techniques[39,40] with improved throughput, this top-down phosphoproteomics strategy that couples functionalized NP-based phosphoprotein enrichment with online LC/MS/MS has the potential to enable a deep coverage and comprehensive characterization of the phosphoproteome for the study of molecular mechanism underlying diseases and the discovery of specific phosphoproteoforms as biomarkers.

Acknowledgements

This research is supported by R01GM117058 (to SJ and YG). YG would also like to acknowledge NIH R01HL096971, R01HL109810 and S10OD018475. We thank Matt Willetts at Bruker for assistance with Data Analysis scripts. We also thank Albert Chen for preparing for heart tissue lysate.

References

1 T. Hunter, *Cell*, 2000, **100**, 113–127.
2 S. J. Humphrey, S. B. Azimifar and M. Mann, *Nat. Biotechnol.*, 2015, **33**, 990–995.
3 S. G. Julien, N. Dubé, S. Hardy and M. L. Tremblay, *Nat. Rev. Cancer*, 2011, **11**, 35–49.
4 R. E. Banks, M. J. Dunn, D. F. Hochstrasser, J. C. Sanchez, W. Blackstock, D. J. Pappin and P. J. Selby, *Lancet*, 2000, **356**, 1749–1756.
5 Z. R. Gregorich and Y. Ge, *Proteomics*, 2014, **14**, 1195–1210.
6 J. Zhang, M. J. Guy, H. S. Norman, Y. C. Chen, Q. G. Xu, X. T. Dong, H. Guner, S. J. Wang, T. Kohmoto, K. H. Young, R. L. Moss and Y. Ge, *J. Proteome Res.*, 2011, **10**, 4054–4065.
7 Y. Peng, Z. R. Gregorich, S. G. Valeja, H. Zhang, W. Cai, Y. C. Chen, H. Guner, A. J. Chen, D. J. Schwahn, T. A. Hacker, X. Liu and Y. Ge, *Mol. Cell. Proteomics*, 2014, **13**, 2752–2764.
8 L. M. Smith and N. L. Kelleher, *Nat. Methods*, 2013, **10**, 186–187.
9 K. Sharma, R. C. D'Souza, S. Tyanova, C. Schaab, J. R. Wiśniewski, J. Cox and M. Mann, *Cell Rep.*, 2014, **8**, 1583–1594.
10 P. H. Huang and F. M. White, *Mol. Cell*, 2008, **31**, 777–781.
11 N. L. Kelleher, P. M. Thomas, I. Ntai, P. D. Compton and R. D. LeDuc, *Expert Rev. Proteomics*, 2014, **11**, 649–651.
12 B. T. Chait, *Science*, 2006, **314**, 65–66.
13 J. C. Tran, L. Zamdborg, D. R. Ahlf, J. E. Lee, A. D. Catherman, K. R. Durbin, J. D. Tipton, A. Vellaichamy, J. F. Kellie and M. Li, *Nature*, 2011, **480**, 254–258.
14 V. Zabrouskov, Y. Ge, J. Schwartz and J. W. Walker, *Mol. Cell. Proteomics*, 2008, **7**, 1838–1849.
15 W. Cai, T. M. Tucholski, Z. R. Gregorich and Y. Ge, *Expert Rev. Proteomics*, 2016, **13**, 717–730.
16 N. Siuti and N. L. Kelleher, *Nat. Methods*, 2007, **4**, 817–821.
17 N. M. Riley and J. J. Coon, *Anal. Chem.*, 2016, **88**, 74–94.
18 L. Xue, W. H. Wang, A. Iliuk, L. Hu, J. A. Galan, S. Yu, M. Hans, R. L. Geahlen and W. A. Tao, *Proc. Natl. Acad. Sci. U. S. A.*, 2012, **109**, 5615–5620.
19 B. Bodenmiller, L. N. Mueller, M. Mueller, B. Domon and R. Aebersold, *Nat. Methods*, 2007, **4**, 231–237.
20 Y. Oda, T. Nagasu and B. T. Chait, *Nat. Biotechnol.*, 2001, **19**, 379–382.
21 J. Porath, J. Carlsson, I. Olsson and G. Belfrage, *Nature*, 1975, **258**, 598–599.
22 S. R. Schmidt, F. Schweikart and M. E. Andersson, *J. Chromatogr. B: Anal. Technol. Biomed. Life Sci.*, 2007, **849**, 154–162.
23 G. Kaur-Atwal, D. J. Weston, P. L. Bonner, S. Crosland, P. S. Green and C. S. Creaser, *Curr. Anal. Chem.*, 2008, **4**, 127–135.
24 L. Hwang, S. Ayaz-Guner, Z. R. Gregorich, W. Cai, S. G. Valeja, S. Jin and Y. Ge, *J. Am. Chem. Soc.*, 2015, **137**, 2432–2435.
25 M. Sytnyk, R. Kirchschlager, M. I. Bodnarchuk, D. Primetzhofer, D. Kriegner, H. Enser, J. Stangl, P. Bauer, M. Voith and A. W. Hassel, *Nano Lett.*, 2013, **13**, 586–593.
26 Z. Gu, X. Xiang, G. Fan and F. Li, *J. Phys. Chem. C*, 2008, **112**, 18459–18466.
27 S. Sun, H. Zeng, D. B. Robinson, S. Raoux, P. M. Rice, S. X. Wang and G. Li, *J. Am. Chem. Soc.*, 2003, **126**, 273–279.
28 B. Bateer, C. Tian, Y. Qu, S. Du, Y. Yang, Z. Ren, K. Pan and H. Fu, *Dalton Trans.*, 2014, **43**, 9885–9891.
29 E. Kinoshita, E. Kinoshita-Kikuta, K. Takiyama and T. Koike, *Mol. Cell. Proteomics*, 2006, **5**, 749–757.
30 R. De Palma, S. Peeters, M. J. Van Bael, H. Van den Rul, K. Bonroy, W. Laureyn, J. Mullens, G. Borghs and G. Maes, *Chem. Mater.*, 2007, **19**, 1821–1831.
31 M.-E. Aubin-Tam and K. Hamad-Schifferli, *Biomed. Mater.*, 2008, **3**, 034001.
32 Y. Pan, X. Du, F. Zhao and B. Xu, *Chem. Soc. Rev.*, 2012, **41**, 2912–2942.
33 Y. Pan, M. J. Long, H.-C. Lin, L. Hedstrom and B. Xu, *Chem. Sci.*, 2012, **3**, 3495–3499.
34 S. Wu, F. Yang, R. Zhao, N. Tolic, E. W. Robinson, D. G. Camp, R. D. Smith and L. Pasa-Tolic, *Anal. Chem.*, 2009, **81**, 4210–4219.
35 J. A. Zhang, X. T. Dong, T. A. Hacker and Y. Ge, *J. Am. Soc. Mass Spectrom.*, 2010, **21**, 940–948.
36 X. W. Liu, Y. Sirotkin, Y. F. Shen, G. Anderson, Y. S. Tsai, Y. S. Ting, D. R. Goodlett, R. D. Smith, V. Bafna and P. A. Pevzner, *Mol. Cell. Proteomics*, 2012, **11**, M111.008524.
37 W. X. Cai, H. Guner, Z. R. Gregorich, A. J. Chen, S. Ayaz-Guner, Y. Peng, S. G. Valeja, X. W. Liu and Y. Ge, *Mol. Cell. Proteomics*, 2016, **15**, 703–714.
38 S. G. Valeja, L. Xiu, Z. R. Gregorich, H. Guner, S. Jin and Y. Ge, *Anal. Chem.*, 2015, **87**, 5363–5371.
39 J. B. Shaw, W. Li, D. D. Holden, Y. Zhang, J. Griep-Raming, R. T. Fellers, B. P. Early, P. M. Thomas, N. L. Kelleher and J. S. Brodbelt, *J. Am. Chem. Soc.*, 2013, **135**, 12646–12651.
40 K. L. Fort, A. Dyachenko, C. M. Potel, E. Corradini, F. Marino, A. Barendregt, A. A. Makarov, R. A. Scheltema and A. J. Heck, *Anal. Chem.*, 2016, **88**, 2303–2310.